View Article Online
View Journal

Dalton Transactions

An international journal of inorganic chemistry

Accepted Manuscript

This article can be cited before page numbers have been issued, to do this please use: S. M. Sheta, S. M. El-Sheikh, D. I. Osman, A. M.S. Salem, O. Ali, F. A. Harraz, W. G. Shousha, M. Shoeib, S. Shawky and D. D. Dionysiou, *Dalton Trans.*, 2020, DOI: 10.1039/D0DT01408G.

ROYAL SOCIETY OF CHEMISTRY

rsc.li/dalton

ROYAL SOCIETY OF CHEMISTRY View Article Online
DOI: 10.1039/D0DT01408G

Journal Name

ARTICLE

Received 00th January 20xx,
Accepted 00th January 20xx

DOI: 10.1039/x0xx00000x

www.rsc.org/

A novel HCV electrochemical biosensor based on a Polyaniline@Ni-MOF nanocomposite

Sheta M. Sheta[1,*], Said M. El-Sheikh[2,*], Diaa I. Osman[3,4], Aliaa M. Salem[2], Omnia I. Ali[4], Farid A. Harraz[2,5], Wafaa Gh Shousha[4], Madiha A. Shoeib[6], Sherif M. Shawky[7,8], Dionysios D. Dionysiou[9]

Hepatitis-C virus ribonucleic acid (HCV-RNA) recognition and quantification based on real-time polymerase chain reaction (RT- PCR) is the main pillar in infection control, management, and response to treatment due to its specificity, sensitivity, and quantification capabilities. However, the high cost, time requirements, and need for sophisticated laboratory infrastructure have limited the use of this method in rapid screening, blood banks, and point-of-care testing (POCT). In this work, a novel label-free electrochemical biosensor constructed using a polyaniline@nickel metal-organic framework (Ni-MOF) nanocomposite was developed for direct detection of unamplified HCV nucleic acid. A robust biosensor was fabricated using smooth layer-by-layer deposition of the polyaniline@Ni-MOF nanocomposite, deoxyribonucleic acid (DNA) probe, and bovine serum albumin (BSA) onto a glassy carbon electrode (GCE) and was subsequently monitored with real-time via cyclic voltammetry (CV) and electrochemical impedance spectroscopy (EIS). The sensitivity and specificity of the newly developed biosensor were specifically examined using the EIS approach. The results revealed that the novel biosensor is highly efficient in quantitative sensing of the HCV target in the presence of nonspecific nucleic acids over the range 1 fM-100 nM with a detection limit of 0.75 fM (at a S/N ratio of 3). To the best of the authors' knowledge, the proposed biosensor is superior to other MOFs platforms. These research findings are expected to have a positive influence on quantitative detection of HCV RNA and other nucleic acids by offering exceptional accuracy and cost effectiveness, especially in low resource countries. Moreover, this biosensor could be simply adopted for full automation and used in point-of-care testing.

Introduction

Infection with the hepatitis-C virus is a serious global health issue. The hepatitis-C virus is distributed worldwide, with various genotypes and subtypes, and the areas of highest prevalence are located primarily in the eastern Mediterranean region (mostly in Egypt). According to the WHO 2017 report, approximately 71,000,000 individuals (1 % of the global population) suffer from chronic HCV infection [1,2]. According to the WHO 2019 HCV fact sheets, almost 399,000 individuals died from HCV infection in 2016 [3,4]. Infection with hepatitis-C virus can progress to liver failure, cirrhosis and eventually hepatocellular carcinoma, thus posing significant health, social and economic challenges to the countries in which it is widespread [5]. Therefore, the WHO has recommended five approaches to eliminate hepatitis by 2030. The most important effort is the development of new diagnostic approaches due to the lack of approved vaccine against HCV. Despite the significant progress made with emerging and notably effective direct-acting antiviral drug (DAA) medications, early and accurate diagnosis remains challenging [6–8]. The unavailability of well-equipped labs for diagnosis and the high cost of analytical tests are some of the main reasons for HCV high mortality and morbidity [9].

Current commercial HCV diagnosis is based on two strategies. (1) The serological strategy includes enzyme-linked immunoassays (ELISA) [10] and electrochemiluminescence (ECL) [11] in addition to the lateral flow rapid test, which all depend on detection of HCV antibodies. The major drawbacks are an inability to detect acute infections and to perform viral RNA quantification. Additionally, these methods cannot be used in screening of immunosuppressant patients or human immunodeficiency virus (HIV) co-infected patients [12]. (2) The second strategy is based primarily on real-time PCR. Due to its specificity and extreme sensitivity, PCR is considered the gold

[1] Inorganic Chemistry Department, National Research Centre, 33, El-Behouth St., Dokki, Giza, 12622, Egypt.
[2] Department of Nanomaterials and Nanotechnology, Central Metallurgical R & D Institute, Cairo, 11421, Egypt.
[3] Clinical Biochemistry Department, National Liver Institute, Menoufia University, Menoufia, 32511, Egypt.
[4] Chemistry Department, Faculty of Science, Helwan University, Cairo, 11795, Egypt.
[5] Promising Centre for Sensors and Electronic Devices (PCSED), Advanced Materials and Nano-Research Centre, Najran University, P.O. Box: 1988, Najran 11001, Saudi Arabia.
[6] Surface treatment &corrosion Control department, Central Metallurgical R & D Institute, Cairo, 11421, Egypt.
[7] Center of Genomics, Helmy Institute, Zewail City of Science and Technology, October Gardens, 6th of October City, 12578, Giza, Egypt.
[8] Biochemistry Department, Faculty of Pharmacy, Misr University for Science and Technology, 6th October City, Giza, 77, Egypt.
[9] Environmental Engineering and Science Program, Department of Chemical and Environmental Engineering (DChEE), University of Cincinnati, Cincinnati, OH 45221-0012, USA.
***Corresponding author:**
S. M. Sheta, E-mail: dr.sheta.nrc@gmail.com, Tel.: +20 1009697356, Fax: +2-02-33370931& Said M. El-Sheikh, selsheikh2001@gmail.com, Phone, +201022316076.
Electronic Supplementary Information (ESI) available: [details of any supplementary information available should be included here]. See DOI: 10.1039/x0xx00000x

standard approach for diagnosis and quantification of viral RNA [13]. Nevertheless, such a test is time consuming, expensive, and labor intensive and requires highly equipped laboratories and sophisticated infrastructure, thus posing significant limitations to POCT settings [4]. Therefore, development of a simple, low-cost diagnostic (without sacrificing sensitivity, specificity and accuracy of the assay) and simple POCT platforms for HCV-RNA detection and quantification is urgently needed for feasible decentralized access, especially in rural areas, to offer better control and management of the infection.

In the last two decades, many attempts have been made to develop simple unamplified HCV-RNA and other nucleic acid assays based on strategies such as Surface Plasmon Resonance (SPR) [14], cell-based methods [15], microfluidics [16], fluorescence [17,18], electrochemical methods [19,20], and electrochemiluminescence [21]. Among the different methods used, electrochemistry techniques have shown superior advantages over the other techniques. This superiority can be attributed to detection and discrimination of the analyte in a complex fluid matrix with high sensitivity and specificity using simple low-cost and low-power devices [22]. For example, a label-free electrochemical assay for direct detection of unamplified HCV RNA was developed based on a thiolated DNA probe immobilized through the Au-S bond on a gold electrode and use of thionine as an electrochemical indicator [23]. Moreover, another HCV-RNA biosensor was reported by Pournaghi-Azar et al. based on adsorption/immobilization of the target DNA probe onto a pencil graphite electrode for HCV 1a genotype identification [24].

Recently, metal-organic frameworks (MOFs) have become an interesting material for or approach to developing nucleic acid-based biosensors, and their success is attributed to their unique properties as tailorable materials with low fabrication cost, large surface area and controllable porosity. In addition, the properties of MOFs offer a high loading capacity for the target NAs probe, thus avoiding degradation and consequently enhancing sensitivity and specificity of NAs detection [25–27]. However, selected MOFs suffer from low electrical conductivity, which creates an obstacle to the design of simple, cost-effective electrochemical (EC)-based NAs biosensors. This obstacle could be overcome via proper design and preparation of composites between MOFs and polymers with good conduction [28,29].

In this study, a novel Ni-MOF was synthesized via a simple method and coupled in situ with conductive polyaniline to yield a Ni-MOF@polyaniline nanocomposite. The as-synthesized composite has high porosity and good electrical conductivity. The nanocomposite was subsequently coated onto the GCE, and the DNA-probe was immobilized on the substrate. The produced structure was treated with a blocking agent, bovine serum albumin (BSA), resulting in high porosity and good electrical conductivity. These properties were confirmed after the formation of nucleic acid double strands between the HCV probe and its target, which led to increased resistance against charge transfer (R_{ct}). Different analytical and spectroscopic tools such as SEM/EDX, FT-IR, UV-Vis/NIR, XRD, XPS, DSC/TGA, mass spectrometry, atomic absorption spectroscopy (AAS), elemental analysis, and magnetometry were used to characterize the as-prepared materials. CV and EIS electrochemical techniques were used to monitor the successful fabrication of the proposed biosensor and detection of the capability of the development. The target biosensor has been successfully used in developing a cost effective, specific and sensitive analytical pathway. Additionally, an effective applicable method has been achieved for direct detection/quantification of unamplified HCV nucleic acid with a low limit of detection of 0.75 fM and a linear dynamic range from 1 fM to 100 nM.

To the best of the authors' knowledge, the current work is the first electrochemical assay for development of a NAs biosensor based on a nanocomposite between MOFs and polyaniline.

Results and discussion

Characterization of Ni-MOF, PA and PA@Ni-MOF nanocomposite

First, the Ni-MOF was synthesized according to the reaction mechanism scheme (Scheme. S1; Supplementary material file) by adding a solution of $NiCl_2.6H_2O$ (2.0 mmol, 0.4754 g) to a flask containing the nanolinker, which was synthesized previously via reflux method by Sheta et al. [30]. Second, the PA was prepared via aniline chemical oxidation polymerization method by David et al. [31]. Whereas, the synthesis of PA@Ni-MOF nanocomposite was adapted by Ramohlola et al. [32], as shown in Scheme. 1a. In the last, the fabrication procedure for the electrochemical HCV biosensor is shown in Scheme. 1b. The most significant spectral and physical data are summarized as follows: melting point (M. P.) >300 °C and Anal/Calcd. (%) for Ni-MOF of $C_{42}H_{58}N_7Ni_4O_{20}$ (1215.73 g/mol): C, 41.49; H, 4.81; N, 8.07. Found: C, 40.95; H, 4.46; N, 7.97. The average of the precipitate yield was 86.8 % after three repetitions of the synthesis process.

(Fig. S1 and Scheme S2; Supplementary material file) show the mass spectrum of the Ni-MOF and the proposed fragmentation, respectively. The theoretically calculated exact mass is 1215.73 g/mol due to the limitation range up to 1100 m/z, which conformed to the formula $C_{42}H_{58}N_7Ni_4O_{20}$. The ion of m/z = 1215.73 g/mol undergoes fragmentation to a stable peak at m/z = 916 (theoretically calculated as 916.39 g/mol) by loss of water and ethanol molecules. The subsequent fragmentations were located at m/z = 696, 475, 223, 165, 149, 108 and 58 (those theoretically calculated were 695.58, 474.76, 222.83, 164.82, 149.15, 108.14, and 59.69 g/mol, respectively). The obtained data were consistent with the suggested structure molecular weight.

The FT-IR spectra (KBr, cm^{-1}) of NL, Ni-MOF, PA and PA@MOF composite are presented in (Fig. S2; Supplementary material file): For Ni-MOF; 3700-3087 ν(H_2O and NH_2); 2934 ν(CH_2); 1630 ν(C=O); 1590-1392 aromatic ν(C=C);1290-776 aromatic ν(CH); 590 ν(Ni–O); 441 ν(Ni–N). For PA, two main peaks appeared at 1505 and 1257 cm^{-1} as ascribed to ν (C-C) and ν(C-N). For the PA@MOF composite: 3704-3036 ν(H_2O and NH_2); 1618 ν(C=O); 559 ν(Ni–O); 476 ν(Ni–N).

View Article Online
DOI: 10.1039/D0DT01408C

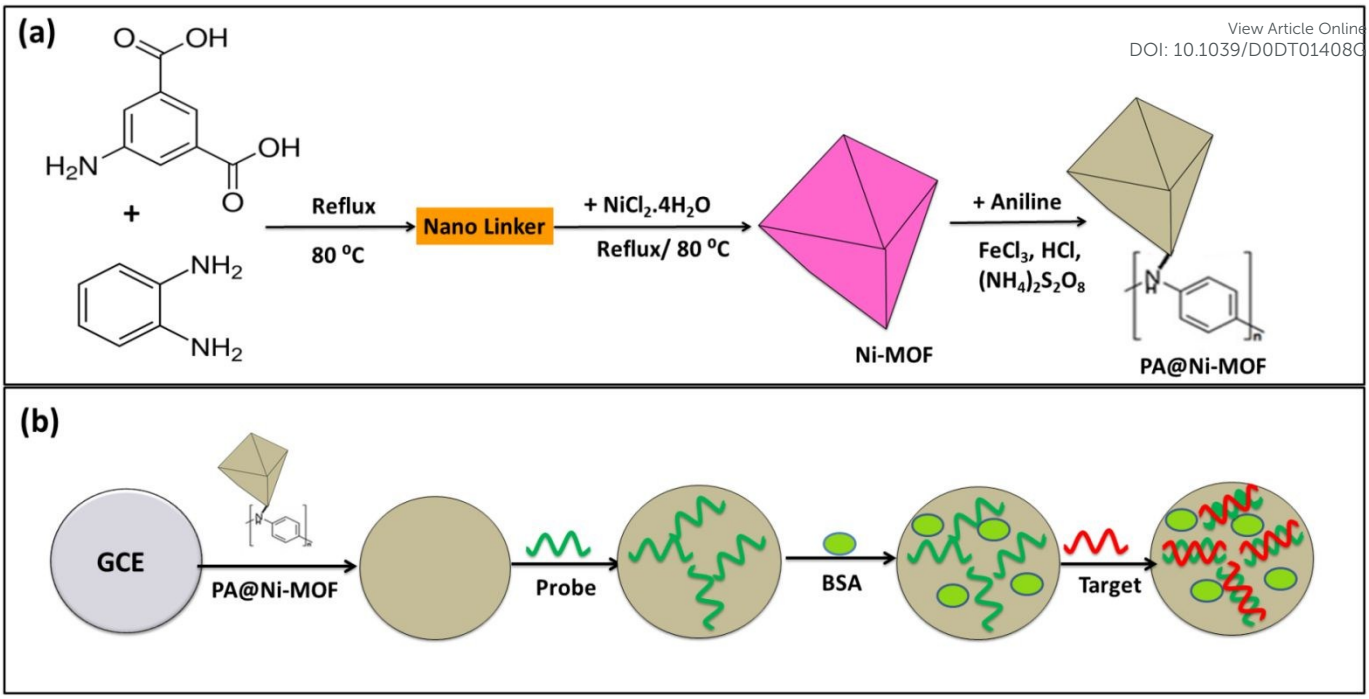

Scheme 1: (a) Schematic diagram of PA@Ni-MOF composite synthesis through chemical oxidation polymerization of aniline monomer in the presence of Ni-MOF, and **(b)** Schematic diagram of the electrochemical HCV- nucleic acid biosensor fabrication

The UV-Vis spectrum (200-2000 nm) and bandgap energy (solid) for NL and Ni-MOF are presented in (Fig. S3a, b, c, and d; Supplementary material file): For NL, λ_{max}= 230, 303 and 386 nm, and the bandgap energy values were approximately 2.0, 2.96, and 3.64 eV. For Ni-MOF, λ_{max}= 236 and 429 nm, and the values of the bandgap energy were approximately 1.92, 2.75 and 3.24 eV. The reduction in the bandgap energy values for Ni-MOF might be due to increased functionalization and conjugation of NL with the amino groups, leading to increases in the band energy of the highest occupied molecular orbital (HOMO) valance, and hence the bandgap energy of Ni-MOF was reduced.

The XRD spectra of the Ni-MOF powder are presented in (Fig. S4; Supplementary material file), which shows that all diffraction patterns were matched with JCPDS card no. 01-1258 and 87-0712 for Ni, card no. 14-0481 for Ni_2O_3 and card no. 73-2058 for carbon. The summary of the XRD data, Millar indices, lattice parameter values, and the interplanar distances of the Ni-MOF were calculated according to the Scherrer equation and are listed in (Table S1; Supplementary material file). From the obtained table data, we note that the XRD spectrum had good agreement with results obtained from the scheme of the mass fragmentation.

The XPS survey scan of Ni-MOF is represented in (Fig. 1 a). The XPS scan obviously shows the peaks of nickel (Ni 2p), carbon (C 1s), nitrogen (N 1s), and oxygen (O 1s). This survey spectrum confirms the existence of the above elements without any impurities in the sample. XPS analysis was applied to inspect four main spectral portions of this sample. Fig. 1b displays the region of C 1s, which reveals spectral peaks at 282.6 and 286.67 eV attributed to C-N and C=O, respectively. In addition, Fig. 1c depicts the region of N 1s and a single signal at 398.0 eV due to the quaternary nitrogen in the sample. Fig. 1d includes the region of O 1s peaks located at 530.98, 531.86 and 533.45 eV. Finally, Fig. 1e shows the region of Ni 2p peaks located at 853.41, 858.0, 870.71 and 872.15 eV. These peaks were attributed to the excitation state core levels from Ni 2p1/2 to Ni 2p3/2 and to the Ni 2p3/2 satellite peak.

The thermogravimetric analysis (TGA) and derivatization of thermal analysis (DTGA) graphs (Fig. 1f) suggested that the Ni-MOF underwent three decomposition steps. The first weight loss of approximately (23.96 %) was due to the expulsion of C_2H_5OH and H_2O molecules at a temperature between 62 to 155 °C. The second weight loss of (58.71 %) was due to the decomposition of phenyl rings at a temperature from 350 to 498 °C. The third stage represented by the Ni and Ni_2O_3 remaining residue was approximately 17.33 %. The TGA data show good compatibility with the above XRD results.

The magnetic hysteresis loop for the Ni-MOF was measured by VSM at (27 °C) and is depicted in (Fig. S5, Supplementary material file). This figure reveals the ferromagnetic behavior of Ni-MOF because the magnetization (Ms) was approximately 0.206 emu/g with a coercivity (Hci) of 425.97 G. and a remanance of 0.01808 emu/g.

FE-SEM images of the Ni-MOF, PA, and PA@Ni-MOF nanocomposite at different magnifications are shown in (Fig. 2). The Ni-MOF (Fig. 2 a, and b) appears to have nano-rod shapes with an average aspect ratio of 0.47 and selected plate sheets. The EDX mapping analysis (Fig. 2c) of Ni-MOF confirmed the presence of building-block elements (C, N, O, and Ni). The EDX analysis is presented in (Table S2, Supplementary material file), and the data had good conformity with the elemental analysis data: C, 41.49; N, 8.07; O, 26.32; and Ni, 19.31. Found: C, 41.80; N, 8.32; O, 30.97; and Ni, 18.91. Furthermore, the PA (Fig. 2 d and e) appeared as an agglomeration of nanosheets. The PA@MOF composite (Fig. 2 f and g) appears to show a porous

structure of aggregated spherical nanoparticles. These results confirmed that the PA@MOF composite was successfully synthesized.

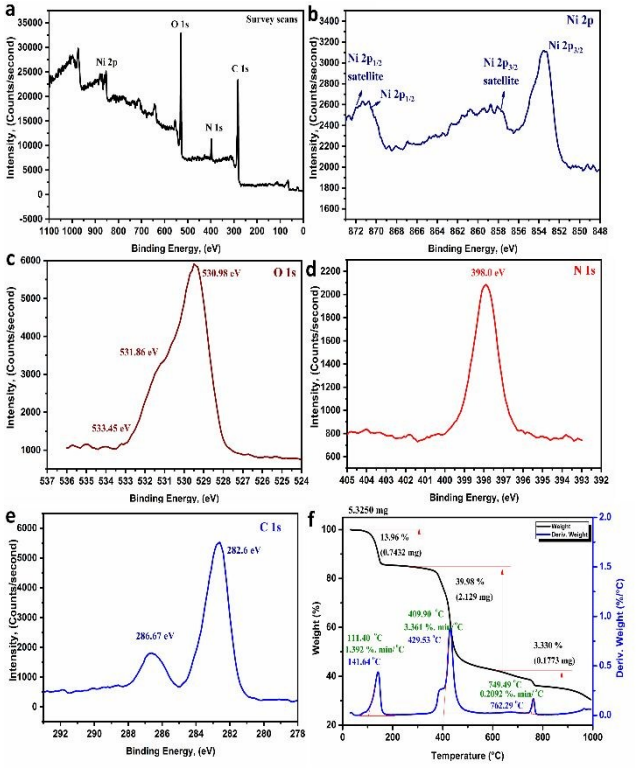

Fig. 1. (a) to (e) The XPS analysis of the Ni-MOF [**(a)** Survey, **(b)** C 1s, **(c)** N 1s, **(d)** O 1s, and **(e)** Ni 2p], **(f)** The thermogravimetric analysis (TGA-DTGA) of the nickel metal–organic framework (Ni-MOF).

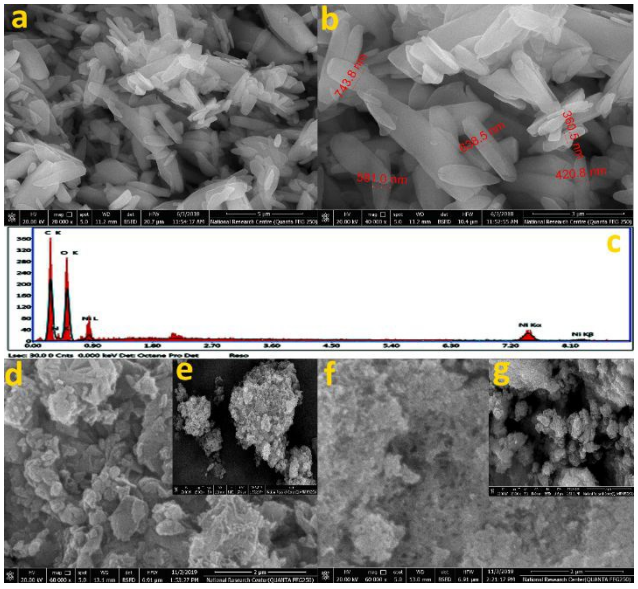

Fig. 2. (a, and b) Field-emission scanning electron microscopy images of the nickel metal–organic framework (Ni-MOF) at different magnification, **(c)** Energy-dispersive X-ray analysis with a single point EDX mapping analysis of Ni- MOF, **(d and e)** FE-SEM images of the polyaniline (PA) at different magnification, and **(f and g)** FE-SEM images of the PA@MOF composite at different magnification.

Based on the obtained spectral and physical analysis of the Ni-MOF, PA and PA@Ni-MOF nanocomposite discussed above, the proposed material structure is approved as shown in the above scheme. In addition to the AAS results that further confirming the presence of PA and MOF in the composite, where it was found that the amount of Ni present in MOF and PA@MOF composite was 24.93 and 0.06 wt %, respectively.

Characterization of electrochemical stepwise construction of the HCV biosensor

CV and EIS are powerful electrochemical techniques that supply evidence of fabrication of the electrochemical biosensor [33,34]. As shown in (Fig. 3a), a couple of clearly defined redox peaks are detected, showing the reversible reduction and oxidation reaction of $[Fe(CN)_6]^{3-/4-}$ on the bare electrode surface (Fig. 3a; curve i). When the PA@MOF composite was cast on the GCE, the peak current of the CV response was enhanced (Fig. 3a; curve ii) due to the high electrical conductivity of the PA@MOF composite. The addition of the capture probe to the electrode was accompanied by a remarkable decrease in the peak current, and this is attributed to the repulsion between the negatively charged phosphate backbone of the probe and the $[Fe(CN)_6]^{3-/4-}$ ions (Fig. 3a; curve iii). Further coating with nonconductive BSA as a blocking agent leads to a further decrease in the peak current (Fig. 3a; curve iv). The presence of the target is associated with a significant decrease in the peak current (Fig. 3a; curve v), and this is attributed to the hybridization ability of the probe with the target forming double strands, and hence, more negative charges and DNA strands were attached to the biosensor. These results demonstrated the successful biosensor design and fabrication, which is supported by the CV and EIS measurements.

EIS was used in further validation of the proposed biosensor in a solution of 5 mM $[Fe(CN)_6]^{3-/4-}$ containing 0.1 M KCl [35]. EIS parameters was carried out at applied potential of + 0.25 V with a 5 mV amplitude and range of frequency from 1 x 10^{-3} to 1 x 10^{-5} HZ. The Nyquist plots of different modified GCEs are displayed in (Fig. 3b). As shown, the linear portion of the curve at lower frequency represents the diffusion process, and the semicircle diameter is equivalent to the charge transfer resistance (R_{ct}). A relatively small semicircle portion was obtained with the GCE (Fig. 3b; curve i), reflecting the slight charge transfer resistance. As shown in (Fig. 3b; curve ii), the coating of the PA@MOF composite on the GCE surface is accompanied by a remarkable decrease in the R_{ct}, suggesting that the PA@MOF composite improved the redox rate on the GCE surface. A remarkable increase in the resistance (Fig. 3b; curve iii) is accompanied by the electrode incubation with the probe, showing that the negative charges of the probe hampered the diffusion of $[Fe(CN)_6]^{3-/4-}$ with respect to the electrode surface [36]. A large semicircle diameter was achieved with the addition of BSA (Fig. 3b; curve iv) because BSA hindered the electron transition. Consequently, as expected, the resistance considerably increased (Fig. 3b; curve v) as a result of incubation with the HCV target (1 pM) for 1 hour, which was attributed to the electrostatic repulsion obtained from the extra-phosphate backbone and negative charges. These data potentially confirmed the effective construction of the intended biosensor as previously designed in the study. Fig. 3c represents the equivalent circuit that fits the impedance spectra. This circuit is composed of the double-layer capacitance (C_{dl}), the

electrolyte resistance (R_s), the Warbury impedance (Z_w), and the charge transfer resistance (R_{ct}).

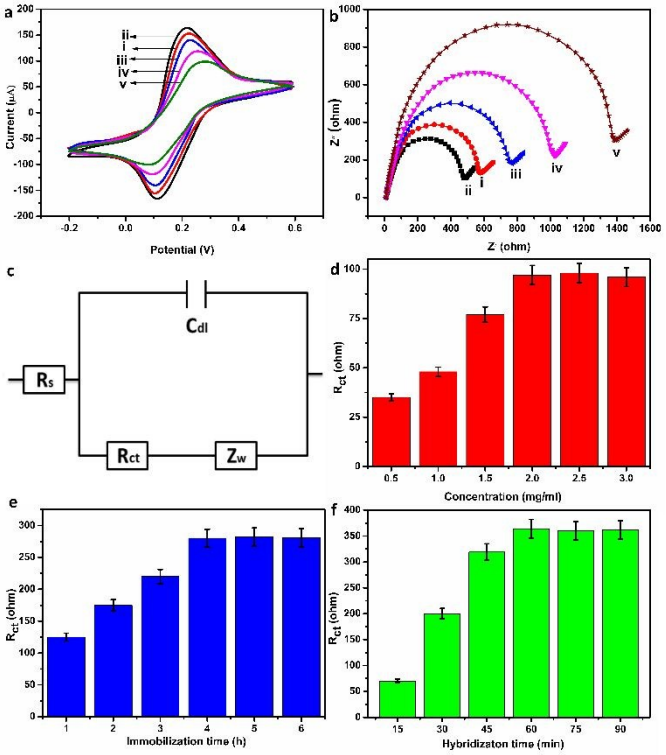

Fig. 3. (a) CV; **(b)** EIS characterization of electrodes at various steps of modification in a 5 mM $[Fe(CN)_6]^{3-/4-}$ solution containing 0.1 M KCl: **(Curve i)** bare GCE, **(Curve ii)** GCE/PA@MOF, **(Curve iii)** GCE/PA@MOF/probe, **(Curve iv)** GCE/PA@MOF/probe/BSA and **(Curve v)** GCE/PA@MOF/probe/BSA/target; **(c)** Represents the equivalent circuit that fits the impedance spectra: C_{dl}, the double-layer capacitance, R_s, the electrolyte resistance, Z_w, the Warbury impedance, and R_{ct}, the charge transfer resistance; **(d)** Effect of the concentration of the PA@MOF composite; **(e)** Effect of the immobilization time of the capture probe on the modified electrode; and **(f)** Effect of the hybridization time between capture probe and its specific target.

Optimization of the experimental parameters

To achieve optimal sensing performance, several parameters were investigated, such as the loading of the PA@Ni-MOF nanocomposite, the immobilization time of the probe and the hybridization time with 1 pM target as a model. As shown in (Fig. 3d), the ΔR represents the difference between the resistance value of the GCE alone and the resistance of the GCE treated with different concentrations of the PA@Ni-MOF composite. The ΔR increased quickly with increased loading of PA@Ni-MOF nanocomposite from 0.5 mg mL^{-1} to 2.0 mg mL^{-1}, followed by a plateau. The highest ΔR was obtained at 2.0 mg mL^{-1}. Consequently, 2.0 mg mL^{-1} was preferred as the best concentration of PA@MOF composite for biosensor construction.

The time of the capture probe immobilization also greatly influences the HCV sensor response. (Fig. 3e) displays the results of investigating the time of the capture probe immobilization. The ΔR increases with increasing probe immobilization time until it reaches a plateau after approximately 4 hours. Thus, 4 hours was preferred as the best immobilization time.

Furthermore, the effect of the hybridization time between the capture probe and the HCV target was also examined to achieve an ideal electrochemical signal. As shown in (Fig. 3f), with an increase in incubation time, the ΔR first increased and subsequently saturated after almost 60 minutes, indicating that the capture probe was completely hybridized to the HCV target. Consequently, 1 hour was chosen as the optimal hybridization time. When the capture probe hybridized with HCV-target, double-strands oligonucleotide are formed on the surface of PA@Ni-MOF nanocomposite, which has been confirmed by measuring the optical density at 260 nm (OD_{260}) before and after the hybridization.

Analytical performance of the HCV electrochemical biosensor

The analytical performance of the proposed electrochemical HCV biosensor was assessed via incubation of the biosensor with various concentrations of the HCV target, and the EIS was used to study the biosensor performance based on $[Fe(CN)_6]^{3-/4-}$ as an EC indicator using the optimum settings. The charge transfer resistance of the HCV biosensor is directly proportional to the concentration of the HCV target, and this is attributed to the electrostatic repulsion between the negatively charged nucleic acid backbone and the electrochemical redox couple indicator $[Fe(CN)_6]^{3-/4-}$. As shown in (Fig. 4a), by increasing the HCV target concentration, the R_{ct} value gradually increases, which is related to the increase of the target-probe hybridization.

As shown in (Fig. 4b), the variation in R_{ct} (ΔR_{ct}) (vs. R_{ct} c=0) of the biosensor was linearly proportional to the logarithm of the HCV target concentration (C_{target}) over the range from 1 fM to 100 nM with a limit of detection (LOD) of 0.75 fM (S/N=3). The linear relationship could be represented by the equation $\Delta R_{ct} = 87.47 \times \log C_{target}$ (fM) + 107.24 with a correlation coefficient of 0.99874. The error bar in the calibration curve has been done through three replications. The results indicate the highly quantitative efficiency of the Ni-MOF-based electrochemical HCV nucleic acid biosensor.

Compared with the reported studies, our proposed HCV biosensor shows great advantages over the analogous NAs biosensors based on probe immobilization through the adsorption method. As shown in Table 1, the proposed method seems to show a good LOD and wider linear range compared with the other analogical detection methods. In addition, our method has a rapid and simple operation. Consequently, it can be concluded that our proposed biosensor displays a remarkable sensitivity and can be used to quantitatively detect HCV-RNA in practical application.

Specificity, stability, and reproducibility of the proposed HCV electrochemical biosensor

To decide whether the proposed HCV biosensor could precisely sense the target with high specificity, the prepared biosensor was incubated with noncomplementary (random) RNA (100 pM) and the fully complementary sequences (target) (10 pM) [37]. As presented in (Fig. 4c), in the presence of noncomplementary RNA, no obvious change was observed in the ΔR, whereas a remarkable increase in ΔR was achieved based on the existence of the complementary target. The conclusion was that the proposed biosensor offered high specificity.

View Article Online
DOI: 10.1039/D0DT01408G

Journal Name

ARTICLE

Table 1. Performance comparison of analogical sensors of our work with recently reported sensors.

Main material	Target	Immob. Method	Detection method	Linear range	LOD	Ref.
AuNPs@MOF	miRNA	Covalent	DPV	1.0 fM - 10 nM	0.35 fM	[20]
Au-electrode	HCV-RNA	Au-SH	CV	0.1 - 2.5 µM	0.02 µM	[23]
Pencil Graphite Electrode	HCV-RNA	Adsorption	DPV	0.1 – 6.0 µM	6.5 nM	[24]
Poly-L-lysine	DNA	Adsorption	DPV	5.0 - 100 nM	4.35 nM	[41]
Graphene/ aminopyrene	DNA	covalent	EIS	1.0 pM - 10 nM	0.45 pM	[42]
polyaniline/rGO	DNA	Adsorption	EIS	1.0 fM - 10 nM	0.25 fM	[43]
Pencil Graphite Electrode	RNA Dengue virus	Adsorption	DPV	10 – 100 nM	3.09 nM	[44]
Polyaniline/ graphene	DNA	Adsorption	EIS	0.1 pM - 1.0 µM	10 fM	[45]
Hemin@MOF	DNA	Covalent	Amperometry	1.0 fM - 10 nM	0.21 fM	[46]
Polyaniline@MOF	HCV-RNA	Adsorption	EIS	1.0 fM- 100 nM	0. 75 fM	The present work

To investigate the stability of the proposed HCV biosensor, we investigated its long-term storage performance [38,39]. The HCV biosensor was stored at 4 °C before use and evaluated periodically. (Fig. 4d) shows the average storage stability over a month. No noticeable changes were observed throughout the first 3 days of storage, and the change in ΔR_{ct} was less than 2.13 %.

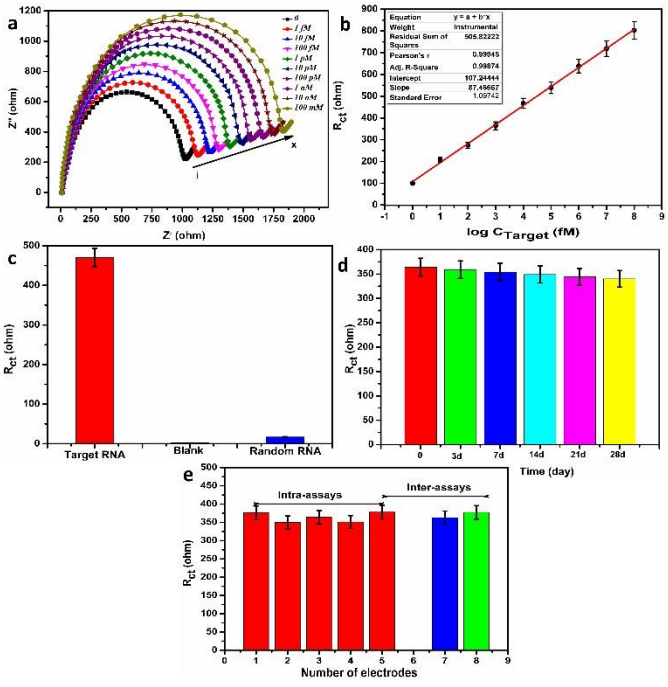

Fig. 4. (a) EIS responses corresponding curves; **(b)** EIS responses of the proposed biosensor incubated with different concentration of HCV target (from a to j): 0,1 fM, 10 fM, 100 fM, 1 pM, 10 pM, 100 pM, 1 nM, 10 nM and 100 nM) in 5 mM $[Fe(CN)_6]^{3-/4-}$ solution containing 0.1 M KCl; **(c)** Specificity of the proposed HCV biosensor toward the blank (zero analyte), target nucleic acid (10 pM), and HCV non-complementary target (100 pM); **(d)** Stability of the biosensor in the presence of 1 pM HCV-nucleic acid target over 28 days; and **(e)** Reproducibility of 7 different electrodes modified with 1 pM HCV target.

After 28 days of storage, the prepared biosensor retained 90.76 % of its initial response to a 1 pM target, which indicates the high stability of the proposed biosensor.

The reproducibility of the assay was evaluated by quantitative detection of the same concentration of HCV target (1 pM) using intra- and interassays (Fig. 4e) [40]. Subsequently, the stability of the modifier material PA@Ni-MOF on the surface of the GCE is greater than or equal to 28 days. The relative standard deviations of the intra-assays and interassays were 3.65 % and 3.27 %, respectively, which confirmed the highly acceptable reproducibility of the proposed HCV biosensor.

Application in real samples

Finally, we investigated and confirmed the applicability of the designed biosensor on serum samples spiked with the HCV target by measuring/detecting the recoveries of the spiked HCV target with three different concentrations (1 pM, 10 pM, and 100 nM) added to 10-fold diluted plasma samples with PBS dilution at a pH of 7.4. The main purpose of our work was to develop a mutation-discriminating RNA sensor that enables the direct analysis of HCV in patient samples. As shown in (Table S3, Supplementary material file), the recoveries ranged from 96.7 % to 99.63 %, and the RSD were in the range of 2.9 % to 4.6 %. These results proved that the prepared HCV biosensor was able to determine the existence of HCV-RNA in real serum samples with no influence on its analytical performance.

Experimental

Materials

See the (Supplementary material file) for material details.

Instruments

See the (Supplementary material file) for material details.

Procedure

Synthesis of nickel metal-organic framework (Ni-MOF)

The nano-linker (NL) was synthesized according to Sheta et al. [30] and is presented in the reaction scheme (Scheme S1-Supplementary material file). The prepared NL was used in the preparation of a novel Ni-MOF. In brief, synthesis of the Schiff base (NL) was achieved by reaction of 5-aminoisophthalic acid (3.0 mmol, 1.0872 g) in ethanol/DMF with 1, 2-phenylenediamine (2.0 mmol, 0.432 g) in ethanol and 1 mL glacial acetic acid, followed by refluxing for 2 days at 80 °C. To this reaction, dissolved $NiCl_2.6H_2O$ (2.0 mmol, 0.4754 g) in H_2O (15 mL) was added in a dropwise manner. The reaction was refluxed at 80 °C for two extra days. Following this process, a light green precipitate was formed, which was filtered, rinsed, and dried.

Polyaniline (PA) synthesis

David et al. previously reported the preparation of PA via a method based on aniline chemical oxidation polymerization [31] with selected modifications. The PA was fabricated as follows: 1 M hydrochloric acid (HCl) solution was split into two equal portions labeled as A and B. In addition, an ice bath was used to adjust the temperature of the solution from 0 to 5 °C. To solution A, monomeric aniline was added. Solution B was used to dissolve ammonium persulfate (APS), which was used as an oxidizing agent. PA synthesis was initiated by dropwise addition of solution B to solution A. After three hours of stirring, a precipitate of PA was formed. The precipitate was filtered and washed several times with distilled water (DI) and ethanol, followed by drying of the obtained powder at 60 °C for 24 hours.

Synthesis of PA@Ni-MOF nanocomposite

The synthesis of PA@Ni-MOF nanocomposite was adapted from [32], as shown in Scheme. 1a. In brief, in a 250 mL round-bottom flask, 1 mL of distilled monomeric aniline containing Ni-MOF (3.6 % wt) was dissolved in a solution of 10 mL HCl/100 mL H_2O followed by stirring at 50 °C for 30 min. Approximately 2.4 grams of ammonium persulfate $(NH_4)2S_2O_8$ and 1.88 grams of $FeCl_3$ were added to the reaction medium. The mixture was stirred at 50 °C for an additional three hours followed by solvent evaporation via placing the solution in an oven at the same temperature overnight. The residual material was rewashed with ethanol and dried again at 50 °C for three hours. In this way, the composite synthesis base on the well-known fact that the transition metal (Ni in the proposed MOF) is forming co-ordination bond with Nitrogen atom in PA. Hence, PA@Ni-MOF has been generated as described above [32].

Construction of the electrochemical HCV biosensor

The applied fabrication procedure for the electrochemical HCV biosensor is shown in Scheme. 1b. Prior to use, the GCE was polished several times with 300 nm and 50 nm alumina slurries on chamois leather. The GCE was subjected to sonication for 5 min in absolute ethanol followed by distilled water. The material was collected and left to dry at room temperature. An amount of 3 µL (concentration of 2 mg/ml) of the above prepared PA@Ni-MOF nanocomposite was cast onto the electrode surface and dried at room temperature. Finally, the prepared electrode was rinsed with distilled water several times and air dried. The prepared electrode was treated with 10 µL of the capture probe (HCV-RNA) (1 µM) for 6 hours at room temperature. The capture probe was immobilized on the composite through electrostatic strong bond between the negatively charged probe backbone and the positively charged NH^{+3} groups of the PA@MOF, with the capture probe nitrogenous bases exposed to the target. Consequently, ensuring that the hybridization with the target occurs at the composite surface not in the solution. Subsequently, the non-immobilized (excess) probe was removed via gentle washing of the prepared electrode with distilled water. Thereafter, the modified electrode was incubated with 3 µL of bovine serum albumin (BSA) (1 mM) solution for 30 min. BSA is a small, moderately non-active protein in many biochemical agents, so it is widely used as a routine blocking agent in most of the biochemical assays that blocks free sites avoiding non-specific binding on the surface and thus, there is no room on the composite surface for it to attach other than on the binding sites of the specific probe.

Finally, the electrode was carefully rinsed with distilled water and prepared for electrochemical measurements (CV and EIS).

Electrochemical measurements

For determination of HCV nucleic acids (NAs), the prepared biosensor (PA@MOF/probe/ BSA@GCE) was hybridized with different concentrations of target HCV for 2 hours to calculate and obtain the optimum time needed for complete hybridization. The PA@MOF/probe/BSA/target@GCE was rinsed with distilled water to eliminate the nonhybridized sequences. Ultimately, all electrochemical measurements were conducted in a solution of 5 mM $[Fe(CN)_6]^{3-/4-}$ containing 0.1 M KCl. The CV measurements were conducted using a potential scan between -0.2 and + 0.6 V vs. the reference electrode at a 50 mV/s scan rate. In addition, EIS was also used in target detection. The HCV target sensing results are presented as the mean value of three parallel independent measurements.

Determination of HCV nucleic acids in real serum samples

Samples from patients (adult males and females) were treated as potentially infectious, according to standard precautions, and were handled properly. Serum was obtained via blood centrifugation for 15 minutes at 4000 rpm, and the separated yellow serum was stored at -20 °C until assay.

Conclusions

In summary, a novel, ultrasensitive and label-free electrochemical nucleic acid biosensor for quantitative determination of unamplified HCV target was fabricated and examined as a model. Biosensor properties such as ease of synthesis, reproducibility, long stability, high sensitivity, accuracy, specificity, and quantification were determined and evaluated. Our proposed method has unique advantages, such as samples do not require labelling or pre-modification by PCR. In addition, our results revealed the biosensor has good selectivity with a notably low limit of detection of 0.75 fM, thus demonstrating a new simple approach for quantitative detection of HCV-RNA as a next step on real clinical samples. To the best of our knowledge, this is the first electrochemical nucleic acid biosensor based on the PA@Ni-MOF nanocomposite. Upon further developments and optimization, the developed biosensor has the potential to compete with RT-

PCR methods and commercial immunoassays for monitoring and management of HCV patients. This method may have potential to be extended to other pathogens such as HIV and such further research could be targeted in the future.

Statement of human and animal rights

The human patient samples used in this study were provided by the Family Medical Laboratory, Ministry of Health, Cairo, Egypt. Informed consent was obtained. The study was approved by the appropriate ethics committee, (Ministry of Health, Cairo, Egypt) and were performed in accordance with ethical standards responsible guidelines of National Hepatology & Tropical Medicine Research Institute registered under no. IRB00003916 in NIH. On the other hand, it was conducted according with ethical standards of the responsible committee on human experimentation (institutional and national) and with the Helsinki Declaration of 1975, as revised in 2000 and 2008 ethical standards. We did not use the samples in any research involving human participants or research involving physical interventions on study participants or involving processing of personal data but conducted the research according to the method described in the article.

Conflicts of interest

There are no conflicts to declare.

Notes and references

1 L. Ti, M. Ng, L. Awendila and P. M. Carrieri, *BMJ Open*, 2019, **8**, 1–4.
2 https://www.who.int/hepatitis/publications/global-hepatitis-report2017/en/-; Last accessed 18/April/2020.
3 E. M. El-Ghitany and A. G. Farghaly, *Heliyon*, 2019, **5**, e02249.
4 https://www.who.int/news-room/fact-sheets/detail/hepatitis-c; Last accessed 18/April/2020.
5 C. Ferri, M. Sebastiani, D. Giuggioli, M. Colaci, P. Fallahi, A. Piluso, A. Antonelli and A. L. Zignego, *World J. Hepatol.*, 2015, **7**, 327–343.
6 J. S. Doyle, E. Aspinall, D. Liew, A. J. Thompson and M. E. Hellard, *Br. J. Clin. Pharmacol.*, 2013, **75**, 931–943.
7 I. Elghitany, *J. High Inst. Public Heal.*, 2019, **49**, 1–9.
8 https://www.who.int/news-room/fact-sheets/detail/hepatitis-c; Last accessed 18/April/2020.
9 J. R. Morgan, M. Servidone, P. Easterbrook and B. P. Linas, *BMC Infect. Dis.*, 2017, **17**, 118–196.
10 A. M. Ibrahim, N. G. M. Abo-el-azaem, M. A. Mohamed, A. Abd-, E. A. Ghaith, S. Hassan, H. Ahmed, M. Mohamed and A. Zaki, *Egypt. J. Hosp. Med.*, 2018, **72**, 4874–4879.
11 C. Bisseye, J. M. N. Ndong, A. M. Matoumba, C. Bengone, G. M. Migolet and B. M. Nagalo, *Asian Pac. J. Trop. Biomed.*, 2017, **7**, 805–808.
12 X. Pei, B. Zhang, J. Tang, B. Liu, W. Lai and D. Tang, *Anal. Chim. Acta*, 2013, **758**, 1–18.
13 M. Y. Lee, J. A. Yang, H. S. Jung, S. Beack, J. E. Choi, W. Hur, H. Koo, K. Kim, S. K. Yoon and S. K. Hahn, *ACS Nano*, 2012, **6**, 9522–9531.
14 X. D. Hoa, A. G. Kirk and M. Tabrizian, *Biosens. Bioelectron.*, 2007, **23**, 151–160.
15 A. G. Venkatesh, H. Brickner, D. Looney, D. A. Hall and E. Aronoff-Spencer, *Biosens. Bioelectron.*, 2018, **119**, 230–236.
16 Y. Zhang and S. Tadigadapa, *Biosens. Bioelectron.*, 2004, **19**, 1733–1743.
17 S. M. Shawky, D. Bald and H. M. E. Azzazy, *Clin. Biochem.*, 2010, **43**, 1163–1168.
18 S. M. Shawky, A. M. Awad, W. Allam, M. H. Alkordi and S. F. EL-Khamisy, *Biosens. Bioelectron.*, 2017, **92**, 349–356.
19 J. Wang, *Biosens. Bioelectron.*, 2006, **21**, 1887–1892.
20 H. Wang, Y. Jian, Q. Kong, H. Liu, F. Lan, L. Liang, S. Ge and J. Yu, *Sensors Actuators, B Chem.*, 2018, **257**, 561–569.
21 Y. Jian, H. Wang, F. Lan, L. Liang, N. Ren, H. Liu, S. Ge and J. Yu, *Microchim. Acta*, 2018, **185**, 1–8.
22 J. Griffin, A. K. Singh, D. Senapati, E. Lee, K. Gaylor, J. Jones-Boone and P. C. Ray, *Small*, 2009, **5**, 839–845.
23 S. Liu, Y. Hu, J. Jin, H. Zhang and C. Cai, *Chem. Commun.*, 2009, **13**, 1635–1637.
24 M. H. Pournaghi-Azar, F. Ahour and M. S. Hejazi, *Electroanalysis*, 2009, **21**, 1822–1828.
25 S. M. Sheta, S. M. El-Sheikh, M. M. Abd-Elzaher and A. R. Wassel, *Appl. Organomet. Chem.*, 2019, **33**, e4777.
26 S. M. Sheta, S. M. El-Sheikh and M. M. Abd-Elzaher, *Dalt. Trans.*, 2018, **47**, 4847–4855.
27 S. M. Sheta, S. M. El-Sheikh and M. M. Abd-Elzaher, *Appl. Organomet. Chem.*, 2019, 33, e5069.
28 S. Carrasco, *Biosensors*, 2018, **8**, 92.
29 D. I. Osman, S. M. El-Sheikh, S. M. Sheta, O. I. Ali, A. M. Salem, W. G. Shousha, S. F. EL-Khamisy and S. M. Shawky, *Biosens. Bioelectron.*, 2019, **141**, 111451.
30 S. M. Sheta, S. M. El-Sheikh, M. M. Abd-Elzaher, M. L. Ghanem and S. R. Salem, *RSC Adv.*, 2019, **9**, 20463–20471.
31 T. David, J. K. Mathad, T. Padmavathi and A. Vanaja, *Polymer*, 2014, **55**, 5665–5672.
32 K. E. Ramohlola, G. R. Monana, M. J. Hato, K. D. Modibane, K. M. Molapo, M. Masikini, S. B. Mduli and E. I. Iwuoha, *Compos. Part B Eng.*, 2018, **137**, 129–139.
33 W. Wang, L. Ge, X. Sun, T. Hou and F. Li, *ACS Appl. Mater. Interfaces*, 2015, **7**, 28566–28575.
34 S. Ge, W. Liu, L. Ge, M. Yan, J. Yan, J. Huang and J. Yu, *Biosens. Bioelectron.*, 2013, **49**, 111–117.
35 L. Bai, Y. Chen, Y. Bai, Y. Chen, J. Zhou and A. Huang, *Biomaterials*, 2017, **133**, 11–19.
36 M. Zhao, Y. Zhuo, Y. Q. Chai and R. Yuan, *Biomaterials*, 2015, **52**, 476–483.
37 P. Zhang, X. Wu, R. Yuan and Y. Chai, *Anal. Chem.*, 2015, **87**, 3202–3207.
38 A. Chen, S. Ma, Y. Zhuo, Y. Chai and R. Yuan, *Anal. Chem.*, 2016, **88**, 3203–3210.
39 Y. Zhang, L. Li, L. Zhang, S. Ge, M. Yan and J. Yu, *Nano Energy*, 2017, **31**, 174–182.
40 S. Ge, F. Liu, W. Liu, M. Yan, X. Song and J. Yu, *Chem. Commun.*, 2014, **50**, 475–477.
41 G. A. Nascimento, E. V. M. Souza, D. S. Campos-Ferreira, M. S. Arruda, C. H. M. Castelletti, M. S. O. Wanderley, M. H. F. Ekert, D. Bruneska and J. L. Lima-Filho, *Biosens. Bioelectron.*, 2012, **38**, 61–66.
42 L. Q. Luo, Z. Zhang, Y. P. Ding, D. M. Deng, X. L. Zhu and Z. X. Wang, *Nanoscale*, 2013, **5**, 5833–5840.
43 T. Yang, Q. Li, X. Li, X. Wang, M. Du and K. Jiao, *Biosens. Bioelectron.*, 2013, **42**, 415–418.
44 N. Oliveira, E. Souza, D. Ferreira, D. Zanforlin, W. Bezerra, M. A. Borba, M. Arruda, K. Lopes, G. Nascimento, D. Martins, M. Cordeiro and J. Lima-Filho, *Sensors*, 2015, **15**, 15562–15577.
45 Q. Zheng, H. Wu, Z. Shen, W. Gao, Y. Yu, Y. Ma, W. Guang, Q. Guo, R. Yan, J. Wang and K. Ding, *Analyst*, 2015, **140**, 6660–6670.
46 G. Yuan, L. Wang, D. Mao, F. Wang and J. Zhang, *Microchim. Acta*, 2017, **184**, 3121–3130.

Journal Name ARTICLE

View Article Online
DOI: 10.1039/D0DT01408G